Since January 2020 Elsevier has created a COVID-19 resource centre with free information in English and Mandarin on the novel coronavirus COVID-19. The COVID-19 resource centre is hosted on Elsevier Connect, the company's public news and information website.

Elsevier hereby grants permission to make all its COVID-19-related research that is available on the COVID-19 resource centre - including this research content - immediately available in PubMed Central and other publicly funded repositories, such as the WHO COVID database with rights for unrestricted research re-use and analyses in any form or by any means with acknowledgement of the original source. These permissions are granted for free by Elsevier for as long as the COVID-19 resource centre remains active.

Results in Chemistry 3 (2021) 100199

Contents lists available at ScienceDirect

Results in Chemistry

journal homepage: www.sciencedirect.com/journal/results-in-chemistry

In silico investigation of phytoconstituents of medicinal herb '*Piper Longum*' against SARS-CoV-2 by molecular docking and molecular dynamics analysis

Shradha Lakhera [a], Kamal Devlal [a], Arabinda Ghosh [b], Meenakshi Rana [a,*]

[a] Department of Physics, School of Sciences, Uttarakhand Open University, Haldwani 263139, Uttarakhand, India
[b] Microbiology Division, Department of Botany, Guwahati University, Guwahati 781014, Assam, India

ARTICLE INFO

Keywords:
SARS-CoV-2
Piper Longum
PL^{pro}
Molecular docking
I-Asarinin

ABSTRACT

Unavailability of treatment for the SARS-CoV-2 virus has raised concern among the population worldwide. This has led to many attempts to find alternative options to prevent the infection of the disease, including focusing on vaccines and drugs. The use of natural products and herbal extracts can be a better option in beating the virus and boosting up immunity. In the present paper, we have done a systematic *in silico* study of papain-like protease of COVID-19 virus with the chemical constituents of herbal plant *Piper Longum*. Screening of the pharmacokinetic properties is done with thirty-two phytoconstituents of *Piper Longum* which help us in selecting the most active components of the plant. After selection molecular docking is performed with Aristololactam ($C_{17}H_{11}NO_4$), Fargesin ($C_{21}H_{22}O_6$), l-asarinin ($C_{20}H_{18}O_6$), Lignans Machilin F ($C_{20}H_{22}O_5$), Piperundecalidine ($C_{23}H_{29}NO_3$), and Pluviatilol ($C_{20}H_{20}O_6$). Molecular dynamic (MD) is also performed with the inhibitor-receptor complex which suggest significant inhibition and a stable complex of I-Asarinin with PL^{pro}. Docking scores and simulation results suggest that I-Asarinin can act as a potential drug like candidate against COVID-19.

1. Introduction

At the present date, no one is unaware or unknown of the 21st century's biggest and most prolonged disaster which had left all the nations helpless. As per the world health organisation (WHO) weekly epidemiological update, over 4.8 million new infected cases and nearly about 86,000 deaths are reported in the May 2021 [1]. Coronavirus is a disease that is caused due to virus and it belongs to the family of severe acute respiratory syndrome (SARS) [2,3]. It is believed that this deadly disease was very first observed in Wuhan, China in late 2019 and jump to humans due to contamination in infected animals including bats [4]. The outbreak of coronavirus disease (COVID-19) is declared a global pandemic and this has to be cured very soon as possible. It can spread due to droplets of an infected person's cough, sneeze, and breathe and they could be in the air or on the surface that you touch [5]. In case the virus is entered into your mucous membrane, within 2 to 14 days your immune system will respond with symptoms like chills, cough, cold, breathing difficulties, muscles aches, headache, loss of smell and, loss of taste, etc. [6]. Till now there have been seven types of human coronavirus demonstrated so far including SARS, Middle East Respiratory Syndrome (MERS), 229E, NL63, OC43, HKU1, and 2019-Novel Coronavirus (nCov) [7]. COVID-19 is more likely to be harmful than a normal virus like common cold as once your lungs become inflamed, it will result in creating troubles in breathing and it may also cause death. This pandemic situation necessitates us to know the structures and function of the virus resulting in COVID-19. To win the fight against this deadly disease, various vaccines have been introduced worldwide. Many vaccines have been demonstrated as being 95% efficient in preventing several symptoms of the COVID-19 virus [8]. Vaccines are done under clinical trials focusing the spike-like protein, nucleic acids, RNA, adenovirus vectors, inactivated viruses, etc. From April 2021, National Regulatory Authority (NRA) have approved twelve vaccines targeting different factors, two for RNA mutant namely Pfizer-BioNTech and Moderna, four for adenovirus vector namely Sputnik V, Oxford-AstraZeneca, J&J, and Convidecia, six for inactivated virus namely Sinopharm (BBIBP), CoronaVac, Covaxin, Sinopharm (WIBP), CoviVac and QazVac and two protein subunit vaccines namely EpiVacCorona and RBD-Dimer for the public use [9]. Food and Drug Administration (FDA) also has approved a variety of drugs for curing COVID-19 like Ivermectin, Doxycycline, Remdesivir, Oseltamivir, Hydroxychloroquine, Favipiravir, and many more [10]. Study of drug-like molecules against proteases of SARS-CoV-2 has been reported for many natural extracts

* Corresponding author.
E-mail address: mrana@uou.ac.in (M. Rana).

https://doi.org/10.1016/j.rechem.2021.100199
Received 30 June 2021; Accepted 15 September 2021
Available online 24 September 2021
2211-7156/© 2021 Published by Elsevier B.V. This is an open access article under the CC BY-NC-ND license (http://creativecommons.org/licenses/by-nc-nd/4.0/).

like curcumin, allicin, and ginger [11], Withania somnifera [12], Indian ginseng [13], Tinospora cordifolia [14] Calendula officinalis [15] and many more. Papain-like protease (PL^{pro}), 3-Chymotrypsin-like protease or main protease ($3CL^{pro}$ or M^{pro}), and spike glycoprotein (S-protein) are common proteases of COVID-19 that are approved by FDA for clinical trials and researchers are focusing on these three viral target proteins of SARS-CoV-2 [16–19]. M^{pro} and PL^{pro} are mainly responsible for dysfunctioning the Ubiquitin and ISG15 from host-cell [20]. Ubiquitin and ISG15 are the amino-acid regulating proteins present in all eukaryotic cells which are responsible for regulating protein in human cells. Targeting PL^{pro} for many antiviral inhibitors might be advantageous in not only preventing viral replication but also resynthesizing the damaged cells by enclosing Ubiquitin and ISG15 back into the host-cell and dysregulating signals in infected cells [21]. Screening of potential drug against protease PL^{pro} is presented for many natural extracts from flavanols [16], neem [22], angelica keiskei (ashitaba), salvia miltiorrhiza, torreya nucifera [23].

In the present study, we have considered an herbal plant *Piper Longum* and performed *in-silico* study with its most active phytoconstituents. The interaction of its phytoconstituents with the PL^{pro} is reported by molecular docking studies and MD simulation. Our results from the present study have established the strong candidature of phytoconstituents of *Piper Longum* to be used as a drug-like molecule for preventing COVID-19 with its wide range of antiviral activity.

2. Materials and methods

2.1. Potential target protein structure for SARS-CoV-2 and protein receptor preparation

Coronavirus exhibits a large number of structural and non-structural polyproteins [24]. The protease PL^{pro} is one of the fundamental enzymes to the coronavirus family consisting of four domains linked with flexible cords which are the fingers domain, palm domain, thumb domain, and Ubiquitin-like (UBL) domain [25]. It imparts in the cleaving of the N-terminal of viral polyprotein which is an important antiviral drug target [26]. Our main target is to dysfunction the replication of PL^{pro}. PL^{pro} also imparts in hydrolysing the peptide bond releasing nsp1, nsp2, and nsp3 proteins [27]. The crystal structure of protease PL^{pro} in complex with non-covalently bonded lead inhibitor 3k and 3j (PDB ID: 4OVZ) and resolution 2.50 Å (Fig. 1) is downloaded from the "Protein Data Bank" (https://www.rcsb.org/) and synthesized with the help of the software "Biovia Discovery Studio Visualizer" (https://disCover.3ds.com/discovery-studio-visualizer-download). The first step of the protein preparation is the removal of the water molecules from the protein. The reason for deleting the water molecules is that if we have water molecules present around the protein's pocket region, the ligand will not comfortably set in the pocket region giving inaccurate results in docking. Polar hydrogens have been added followed by energy minimization in the torsional space and Kollman charges have also been added to the protein. All the heta-atoms present in the protein are also removed as they are unusual residues of DNA, RNA, proteins, and other atoms which can jam the binding sites and create trouble in protein–ligand binding. The output structure of the macromolecule is then saved in pdbqt format.

2.2. Potential inhibitor: Piper Longum

For the present work, we have chosen the medicinal plant *Piper Longum* or Piper, or sometimes called Indian long pepper (Fig. 2). *Piper Longum* is the native of the Indian subcontinent and is also found in Asia and European land. It belongs to the family of Piperaceae and has a strong taste resemblance with *Piper nigrum* which is also a member of same family [28]. It is a flowering vine with each part of it being significantly use, the most important spice in Indian foodstuffs, and are mainly cultivated in India for its fruit. Somehow, its leaves also play a vital role in medical science and is used as a preventive measure for many viral diseases like cancer, inflammation, depression, diabetes, obesity, and hepatotoxicity [29–31]. Along with anti-viral property, *Piper Longum* also has significant pharmacological activities including anticancer, immunomodulatory, cardioprotective, antimicrobial, antifungal, bioavailability-enhancing, antioxidant [32,33]. *Piper Longum* is known to increase the total white blood cells (WBC) count to 142.8 and 138.9% which is responsible for boosting immunity [34]. The selection of *Piper Longum* is motivated by the fact that symptoms of the COVID-19 are very common to normal cough and cold problems in which *Piper Longum* is preferred as a cure ailment. The usage of the plant began in the sixteenth century [35] and is very highly beneficial in curing chronic bronchitis, asthma, constipation, paralysis of the tongue, cholera, chronic malaria, viral hepatitis, respiratory infections, stomach ache, bronchitis, diseases of the spleen, cough, and cancers. With the help of the online database "Indian Medicinal Plants Phytochemistry and Therapeutics" (IMPPAT) (https://cb.imsc.res.in/imppat/home), thirty-two phytoconstituents of *Piper Longum* were traced and their structures were downloaded from the online database "PubChem" (https://pubchem.ncbi.nlm.nih.gov/) in SDF format.

Later the structures of phytochemicals were converted into PDB format with the help of graphic user interface "Open Babel GUI" (http://

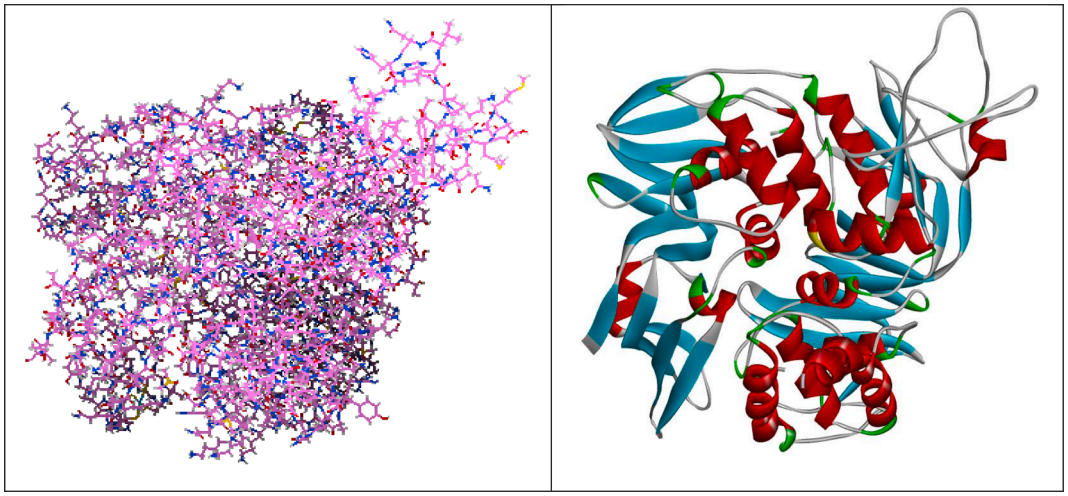

Fig. 1. (a) Target protein: PL^{pro} (PDB ID: 4OVZ) with removed water molecules and with added polar hydrogens and kollman charges (b) Structure of Human Coronavirus Papain-Like Protease PL^{pro} (PDB ID: 4OVZ) with lead inhibitor.

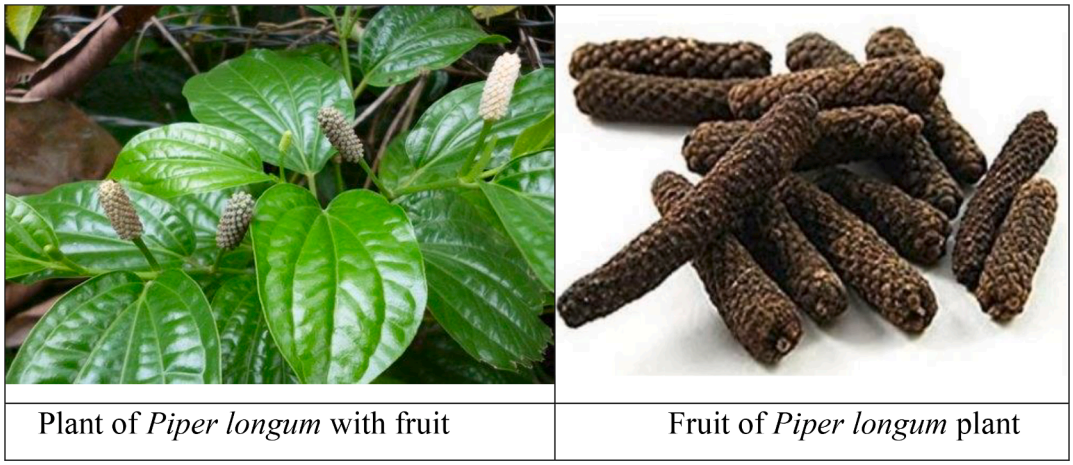

Fig. 2. Morphology of *Piper Longum.*

openbabel.org/wiki/Main_Page) [36]. We have performed molecular docking with Aristololactum, Fargesin, I-Asarinin, Lignans Machilin F, Piperundecalidine and Pluviatilol. 3-D structures of all the selected phytoconstituents are downloaded from PubChem and shown in Table 1 along with their PubChem id.

Table 1
Different phytoconstituents extracted from *Piper Longum* with 3-D structure and PubChem ID.

Compound name with symbol	Database ID	Three-dimensional structure
Aristololactam ($C_{17}H_{11}NO_4$)	PubChem ID 96710	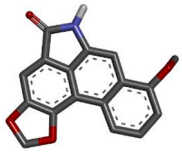
Fargesin ($C_{21}H_{22}O_6$)	PubChem ID 10926754	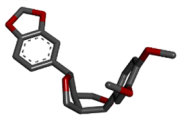
l-asarinin ($C_{20}H_{18}O_6$)	PubChem ID 11869417	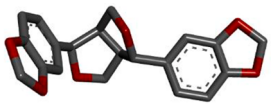
Lignans Machilin F ($C_{20}H_{22}O_5$)	PubChem ID 13844301	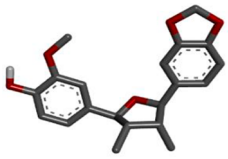
Piperundecalidine ($C_{23}H_{29}NO_3$)	PubChem ID 44453654	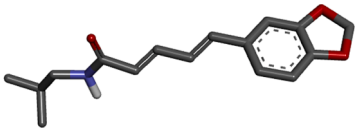
Pluviatilol ($C_{20}H_{20}O_6$)	PubChem ID 70695727	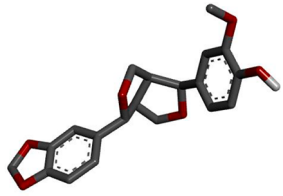

2.3. Drug-likeness properties and ADMET properties

A set of rules and guidelines for determining the structural properties is preferred for initial screening of drug-likeness of compound. Some such Drug-likeness rules are Lipinski's rule, MDDR-like rule, Veber's rule, Ghose filter, Egan rule, Muegge rule, Lipophilicity (iLOGP, WLOGP, XLOGP3, MLOGP, Log Po/w), water solubility (Log S (SILICOS-IT)), etc. [37]. According to Lipinski's rule (Pfizer's rule or simply the rule of five (RO5)), any chemical compound can be used as an orally active drug if and only if it will not violate that set of rules [38]. The compounds which simply obey RO5 will have more chances for being orally used for human consumption and reach the markets. The mentioned rules preliminarily justify whether the compound is ideal for drug synthesis or not. Some of the rules like molecular weight < 500, hydrogen-bond donors < 5, hydrogen-bond acceptor < 10, MLOGP (n-octanol–water partition coefficient) < 4.15, molar refractivity should be between 40 and 130, log P ranging between -0.4 to $+5.6$, solubility (log S) > -5.7, also help us to preliminary test the suitable drug molecule [39]. All these preclinical tests help in differentiating between drug-like and non-drug-like structures. All these properties are studied with the help of the online software SWISS-ADME (http://www.swissadme.ch/). This software facilitates us to analyse all the physiochemical properties, medicinal chemistry, drug-likeness properties, pharmacokinetics, lipophilicity, etc. In virtual screening of drug-likeness properties, it is often seen that several approved drugs do not follow all the screening rules completely thus violating any of the RO5 and other drug-likeness rules [40]. Drugs like Dabigitran used for preventing blood clots, Bromocriptine used for preventing pituitary tumors, Medoxomil used for preventing hypertension, etc. are a few medicines that are available in markets for human consumption even although they violate two RO5 rules [40]. Atazanavir, the most commonly used drug for the treatment of human immunodeficiency virus (HIV-AIDS), violates three of the RO5 rules but still, it is a very preferred antiretroviral protease inhibitor [41]. Lapatinib and Nilotinib are very popular tyrosine kinase inhibitors preferred for regulating many cellular functions but RO5 rules are violated by both of them [42]. Even, Remdesivir, the most used medicine in this pandemic also violates two of the RO5 rules due to its molecular weight of 602.6 (exceeding 500) and H-bond acceptor count of 13 which exceeds the rule's limit of 10 [43]. If we go through all these facts, we conclude that despite the violation of few drug-likeness rules, drugs are preferred manually. Phytochemicals we have considered as potential inhibitors against PL^{pro} protease, are so likely to follow all these rules, although some of them may violate but validate other rules.

Along with the RO5 and other pharmacokinetic rules, the considered inhibitor must follow the ADMET properties. "Absorption" reveals the journey of the drug throughout our body, "Distribution" is about the

transfer of drug from one location (organ) to another, "Metabolism", is a set of chemical reactions which drug undergo during the journey after metabolism is done, the drug should be eliminated from any part of the body in any form like sweat, urine, excrete, etc., called "Excretion" and "Toxicity" is the degree to which a drug can damage an organism [44]. The ADMET features are listed using ADMETsar (http://lmmd.ecust.edu.cn/admetsar1) open-source tool. In computational drug discovery, subcellular localization of a receptor plays a vital role in improving target identification. It reveals which intercellular part of protein localizes the drug and undergoes the drug action. For all the ligands, the subcellular localization is Mitochondria. Pan-assay interference compounds (PAINS) are the compounds that should be necessarily eliminated from the target protein due to their tendency of giving false positive results while predicting the binding site [45]. Suppose our drug-like molecule targets at some binding site (say A), PAINS will automatically bind it with other binding sites giving false results. A few common PAINS are toxoflavin, isothiazolones, curcumin, enones, hydroxyphenyl hydrazones, quinones, and many more [46]. Plasma protein binding is said to be an important factor in the screening and drug discovery process as it shows the capability of our drug to bind with the protein within the blood and Acute oral toxicity is referred to all the reactions that happened to the human body after the consumption of the drug. For all the considered ligands, AOT falls in the 3rd category among 4 categories. As per the United States Environmental Protection Agency (US EPA), compounds are classified into four categories based on their LD50 values (lethal dose). Compounds falling in the first category have LD50 < 50 mg/kg, in second category LD50 value, should fall between 50 and 500 mg/kg, third category have LD50 value between 500 and 5000 mg/kg.

2.4. Molecular docking and visualization

In computer-assisted drug designing, molecular docking is considered as the molecular modelling tool that is preferred for the prediction of the ligand-receptor interaction when both the molecules are bound together to form a stable complex [47]. In this work, we have used "Auto Dock Vina" software (http://vina.scripps.edu/) for performing molecular docking [48]. The algorithm of Auto Dock vina for docking of 4OVZ deals with configuration parameters like nine binding modes, exhaustiveness = 8, energy difference = 4 kcal/mol, grid box with center coordinates x = −9.665, y = 40.995, z = −30.003 of the position of the target protein is used to do the docking-based studies on the suggested inhibitor onto the protease of coronavirus. The synthesized protein is saved in pdbqt format. Similarly, ligands are also synthesized with the help of Auto Dock vina and saved in pdbqt format. Out of all the nine output poses obtained, the most stable receptor-ligand complex is selected based on the analysis of different parameters. These parameters are binding affinity (G) (Kcal\mol), dipole moment of ligand (in Debye), number of H-bonds, and drieding energy. To verify our docking scores, we have performed docking for the same protein–ligand pairs with the help of another docking software Pyrx (https://sourceforge.net/projects/pyrx/files/latest/download) [49].

2.5. Molecular dynamics

MD simulations are performed for the best-docked complex, to study its stability and physical movements [50]. The simulation is done with the help of software the Desmond modules vs 2020.1. For protein–ligand docked complex, OPLS2005 force field was applied to provide a larger coverage of organic functionality. 11 Na^+, and 8 Cl^- counter ions are added to neutralize the charges and simple point charge (SPC) is also used to fetch correct density and permittivity. The system should be close to mimic the human physiological condition for which 0.15 M NaCl salt concentrations are added. MD Simulation continued till 100 ns at the conditions of Isothermal-Isobaric ensemble (constant number of particles, pressure, temperature) (NPT). Simulation interaction diagrams are studied with the help of the Desmond GUI tool Maestro. Parameters obtained in the simulation like root-mean square deviation (RMSD), root mean square fluctuation (RMSF), number of H-bonds, radius of gyration, and calculated binding energy which helps us to predict the stability of the complex [49]. The calculation of binding energy of the protein–ligand docking complexes was estimated with the help of MM/GBSA and is done by the below-given equation.

$$\Delta G_{binding} = G_{docking\ complex} - -\left(G_{protein} + G_{ligand}\right) \quad (1)$$

Where, $\Delta G_{binding}$ is binding free energy and $G_{docking\ complex}$, $G_{protein}$, and G_{ligand} are the free energies of the docking complex, protein and ligand, respectively.

3. Results and discussions

3.1. Virtual screening result analysis

After the computer-based screening of the inhibition properties of 32 phytochemicals of *Piper longum*, we have observed that some compounds were near about to show drug-likeness properties. Among all the phytochemicals, the most drug likely compounds are selected. These compounds are Aristololactam, Fargesin, I-Asarinin, Lignans Machilin F, Piperundecalidine, and Pluviatilol. These compounds follow most of the drug-likeness rules and ADMET properties. All these components follow RO5 completely without even a single violation. Molar refractivity for all these chemicals is between 40 and 130, have molecular weight <500, all have a total number of atoms >20 and all have log p values between −0.4 to 5.6 which shows that they follow the Ghose filter completely (Table 2).

In our case, the considered phytochemicals do not reveal the presence of any PAINS and also show moderate solubility in water and high gastrointestinal absorption. Blood brain barrier penetration is also high for all these components which is a very important feature of any drug. In the human body, epithelial cell line formed from Caco-2 cell can be used to predict in vivo absorption of drugs and for which all of the selected phytoconstituents show positive results [51]. The phytoconstituents we have selected shows 100% P-P binding which shows fine binding of drug-like molecule with protein in blood [52]. The Ames test is used to determine whether the chemical is mutagenic and can also revert mutations in the DNA of an organism and restore its ability to synthesize growth leading essential amino acids [53]. In our case, the compounds show nontoxicity in the Ames test. Not any of the selected phytoconstituents promotes carcinogenicity. Carcinogenicity is the toxic property of any chemical, any radionuclide, or any radiation that shows its ability or tendency to produce cancers. Compounds having toxic dose TD50 < 10 mg/kg of body's weight per day are assigned as danger, TD50 > 10 mg/kg of body's weight per day are assigned as moderate/warning and non-carcinogenic chemicals are the one with zero risk of causing cancer as like in our case. Inhibitor that confirms the RO5 rules and other Drug-likeness rules have the high chances of being prioritized for the clinical trials and have shown their strong candidature as a potential drug against protease PL^{pro} of COVID-19. Similarly, ADMET properties mentioned in Table 3, are mostly followed by the selected phytochemicals.

3.2. Molecular docking result analysis

To get the variation in binding affinity score corresponding to each ligand, docking for every single ligand have been performed several times. The most stable inhibitor-receptor (protein–ligand) structure is selected based on minimum binding affinity score, drieding energy, and maximum dipole moment. Interactions between these compounds and target proteins by forming conventional, pi-donor and carbon H-bonds are shown in Table 4. with common active site amino acid residues Leucine (LEU), Glutamine (GLN), Threonine (THR), Lysine (LYS),

Table 2
Molecular configuration and Drug-likeness properties of proposed ligand drug molecules against COVID-19 (Data collected from SWISS ADME).

Name of Ligand	Aristololactum	Fargesin	I-Asarinin	Lignans Machilin F	Piperundecalidine	Pluviatilol
Physiochemical Properties						
Molecular weight (g/mol)	293.27	370.40	354.4	342.39	367.48	356.37
Hydrogen-bond Donor count	1	0	0	1	0	1
Hydrogen-bond Acceptor count	4	6	6	5	3	6
Rotatable Bond Count	1	4	2	3	9	3
TPSA ($Å^2$)	60.55	55.38	55.38	57.15	38.77	66.38
Heavy Atom Count	22	27	26	25	27	26
Molar Refractivity	83.32	96.92	90.00	93.48	113.84	92.45
Lipophilicity						
Log $P_{o/w}$ (iLOGP)	2.51	3.67	3.46	3.35	4.72	3.25
Log $P_{o/w}$ (XLOGP3)	3.12	2.81	2.68	3.93	5.78	2.48
Log $P_{o/w}$ (WLOGP)	3.01	2.86	2.57	3.57	4.62	2.56
Log $P_{o/w}$ (MLOGP)	2.42	1.79	1.98	2.38	3.66	1.57
Log $P_{o/w}$ (SILICOS-IT)	4.20	3.48	3.25	3.49	5.58	2.96
Consensus Log $P_{o/w}$	3.05	2.92	2.79	3.34	4.87	2.56
Water Solubility						
Log S (SILICOS-IT)	−5.99	−5.09	−4.60	−4.89	−4.66	−4.39
class	Moderately soluble	Moderately soluble	Moderately soluble	Moderately soluble	Moderately soluble	Moderately soluble
Solubility	2.99e-04 mg/ml; 1.02e-06 mol/l	3.03e-03 mg/ml; 8.18e-06 mol/l	8.98e-03 mg/ml; 2.54e-05 mol/l	4.44e-03 mg/ml; 1.30e-05 mol/l	8.04e-03 mg/ml; 2.19e-05 mol/l	1.44e-02 mg/ml; 4.03e-05 mol/l
Pharmacokinetics						
GI absorption	High	High	High	High	High	High
Log K_p (skin permeation)	−5.87 cm/s	−6.56 cm/s	−6.56 cm/s	−5.60 cm/s	−4.44 cm/s	−6.71 cm/s
Drug-likeness						
Lipinski Rule	Yes; 0 violation	Yes; 0 violation	Yes; 0 violation	Yes; 0 violation	Yes; 0 violation	Yes; 0 violation
Ghose Filter	Yes	Yes	Yes	Yes	Yes	Yes
Veber (GSK) Rule	Yes	Yes	Yes	Yes	Yes	Yes
Egan (phatmacial) Filter	Yes	Yes	Yes	Yes	Yes	Yes
Muegge (Bayer) Filter	Yes	Yes	Yes	Yes	No; 1 violation: XLOGP3 > 5	Yes
Bioavailability	0.55	0.55	0.55	0.55	0.55	0.55
Medicinal Chemistry						
PAINS	0 alert	0 alert	0 alert	0 alert	0 alert	0 alert
Brenk	1 alert: polycyclic aromatic hydrocarbon 3	0 alert	0 alert	0 alert	2 alerts: Michael acceptor 1, polyene	0 alert
Lead-likeness	Yes	No; 1 violation: MW > 350	No; 1 violation: MW > 350	No; 1 violation: XLOGP3 > 3.5	No; 3 violations: MW > 350, Rotors > 7, XLOGP3 > 3.5	No; 1 violation: MW > 350
Synthetic accessibility	2.56	4.30	4.12	4.13	3.53	4.19

Table 3
ADMET properties of screened phytochemicals of drug molecule (Data collected by ADMETsar database).

Name of Ligand	Aristololactum	Fargesin	I-Asarinin	Lignans Machilin F	Piperundecalidine	Pluviatilol
Absorption						
Human Intestinal Absorption	HIA+	HIA+	HIA+	HIA+	HIA+	HIA+
Blood Brain Barrier	BBB+	BBB+	BBB+	BBB+	BBB+	BBB+
Caco-2 permeable	Caco2+	Caco2+	Caco2+	Caco2+	Caco2+	Caco2+
P-glycoprotein substrate	Non-substrate	Non-substrate	Non-substrate	Non-substrate	Non-substrate	Non-substrate
P-glycoprotein inhibitor	Non-inhibitor	inhibitor	Non-inhibitor	inhibitor	Non-inhibitor	Non-inhibitor
Distribution						
Plasma Protein Binding (PP)	0.918; 100%	0.668; 100%	0.632; 100%	1.031; 100%	1.078; 100%	0.737; 100%
Metabolism						
CYP450 2C9 substrate	Non-substrate	Non-substrate	Non-substrate	Non-substrate	Non-substrate	Non-substrate
CYP450 2D6 substrate	Non-substrate	Non-substrate	Non-substrate	Non-substrate	Non-substrate	Non-substrate
CYP450 3A4 substrate	substrate	Non-substrate	Non-substrate	substrate	Non-substrate	Non-substrate
CYP450 1A2 inhibitor	Inhibitor	Inhibitor	Inhibitor	Inhibitor	Inhibitor	Inhibitor
CYP450 2C9 inhibitor	Inhibitor	Inhibitor	Inhibitor	Inhibitor	Inhibitor	Inhibitor
CYP450 2D6 inhibitor	Non-Inhibitor	Inhibitor	Inhibitor	Inhibitor	Non-Inhibitor	Inhibitor
CYP450 2C19 inhibitor	Inhibitor	Inhibitor	Inhibitor	Inhibitor	Inhibitor	Inhibitor
CYP450 3A4 inhibitor	Inhibitor	Inhibitor	Inhibitor	Inhibitor	Non-Inhibitor	Inhibitor
Toxicity						
Ames test	Non toxic	Non toxic	Non toxic	Non toxic	Non toxic	Non toxic
Carcinogenicity	Non-carcinogens	Non-carcinogens	Non-carcinogens	Non-carcinogens	Non-carcinogens	Non-carcinogens
Biodegradation	biodegradable	Non-biodegradable	Non-biodegradable	Non-biodegradable	biodegradable	Non-biodegradable
Acute Oral Toxicity	0.918 kg/mol	1.518 kg/mol	1.189 kg/mol	2.589 kg/mol	2.032 kg/mol	1.424 kg/mol

Table 4
Interaction details of the best pose for different ligands: Aristololactum, Fargesin, I-Asarinin, Lignans Machilin F, Piperundecalidine, Pluviatilol with receptor protein 4OVZ.

Protein	Binding affinity (kcal/mol)	Hydrogen-bonded interaction (donor: acceptor, distance in A) [Type of bond]	Total number of Hydrogen-bonds	Dipole moment (Debye)	Dreiding energy (protein + ligand)
Aristololactam					
4OVZ	−9.5	A:LEU76:HN - : UNL1:O; 2.4819 [Conventional Hydrogen-bond] A:GLN175:HE21 - :UNL1:O; 2.9367 [Conventional Hydrogen-bond] A:GLN175:HE22 - :UNL1:O; 2.7182 [Conventional Hydrogen-bond] B:LEU76:HN - : UNL1:O; 2.2026 [Conventional Hydrogen-bond] 5. B:GLN175: HE22 - :UNL1:O; 3.0655 [Conventional Hydrogen-bond]	5	2.249	116.84
Fargesin					
4OVZ	−8.5	A:LYS158:HZ3 - : UNL1:O; 2.9368 [Conventional Hydrogen-bond] B:GLN233:HE22 - :UNL1:O; 2.2549 [Conventional Hydrogen-bond] UNL1:C - A: GLN270:O; [Carbon Hydrogen-bond] UNL1:C - B: MET209:O; 3.26958 [Carbon Hydrogen-bond] UNL1:C - A: TYR269:O; 3.66837 [Carbon Hydrogen-bond]	5	4.265	167.12
I-Asarinin					
4OVZ	−10.8	B:THR75:HG1 - : UNL1:O; 2.5002 [Conventional Hydrogen-bond] B:ASN157: HD22-:UNL1:O; 2.5107 [Conventional Hydrogen-bond] B:HIS176:HD1 - : UNL1:O; 2.3831 [Conventional Hydrogen-bond] UNL1:C - B: ASP77:OD2; 3.6037 [Carbon Hydrogen-bond] B:HIS176:HE2 - : UNL1; 3.2873 [Pi-Donor Hydrogen-bond] A:LEU76:HN - : UNL1;3.10226 [Pi-Donor Hydrogen-bond]	6	3.901	135.39
Lignans Machilin F					
4OVZ	−9.5	A:ASN110: HD21:UNL1: O;2.50568 [Conventional Hydrogen-bond] A:ASN110: HD22:UNL1: O;2.4572 [Conventional Hydrogen-bond] A:ASN110: HD22:UNL1: O;2.7530 [Conventional Hydrogen-bond] A:THR159:HG1: UNL1:O;2.4699 [Conventional Hydrogen-bond] B:GLN233:HE22- :UNL1;2.8227 [Pi-Donor Hydrogen-bond]	5	4.988	129. 51
Piperundecalidine					
4OVZ	−8.5	A:LEU76:HN - : UNL1:O; 2.3967 [Conventional Hydrogen-bond] B:GLN175:HE22 - :UNL1:O; 2.7465 [Conventional Hydrogen-bond] B:HIS176:CE1 - : UNL1:O; 3.4737 [Carbon Hydrogen-bond] UNL1:C - A: TYR155:O; 3.3326 [Carbon Hydrogen-bond]	4	2.827	132.32
Pluviatilol					
4OVZ	−9.6	B:HIS74:HD1-: UNL1:O; 2.6959 [Conventional Hydrogen-bond] B:LEU76:HN - : UNL1:O; 3.0193 [Conventional Hydrogen-bond] B:ASN157:HD22 - :UNL1:O; 2.5886 [Conventional Hydrogen-bond] B:HIS176:HE2 - : UNL1:O; 2.2937 [Conventional Hydrogen-bond] UNL1:H - B: TYR155:O; 2.2595 [Conventional Hydrogen-bond]	8	4.714	142.38

(*continued on next page*)

Table 4 (*continued*)

Protein	Binding affinity (kcal/mol)	Hydrogen-bonded interaction (donor: acceptor, distance in A) [Type of bond]	Total number of Hydrogen-bonds	Dipole moment (Debye)	Dreiding energy (protein + ligand)
		B:THR75:CA - : UNL1:O; 3.1926 [Carbon Hydrogen-bond] UNL1:C-B: GLN175:OE1; 3.5851 [Carbon Hydrogen-bond] A:LEU76:HN - : UNL1; 3.1714 [Pi-Donor Hydrogen-bond]			

Asparagine (ASN), Histidine (HIS), Tyrosine (TYR), Methionine (MET) and Aspartic acid (ASP). Dreiding energy is also reported for different poses which accounts for additive energy of complex under energy components like bond length, angles, etc.

The selection of the best poses for all the considered phytochemicals is done based on minimum binding affinity score. Thus, pose 2 of Aristololactum having a binding affinity score of −9.5Kcal/mol, five H-bonds, and drieding energy of 116.88 (SD1) is selected as the best pose. Pose 4 of Lignan Machilin F with the same binding affinity score as of Aristololactum, the maximum binding affinity score of 4.988 Kcal/mol and five H-bonds (visit SD2) is selected as the best pose. In the case of Fargesin and Piperundecalidine, pose 9 and pose 3 both with the same binding affinity score of −8.5Kcal/mol, minimum drieding energies of 167.12 and 132.32 and five and four H-bonds (visit SD3 and SD4), are selected as the best poses respectively. For I-Asarinin, the compound with best binding affinity score of −10.8 kcal/mol among all the phytochemicals, first pose is selected as the best pose. Along with best binding affinity score, it also has a maximum H-bond number six. For Pluviatilol pose 3 with binding affinity score −9.6Kcal/mol, eight H-bonds, and drieding energy 142.38 is the best-preferred pose among all nine (visit SD5). 2D and 3D structures of the selected poses of ligands found in the active binding sites of 4OVZ protein for Aristololactum, Lignan Machilin F, Fargesin, Piperundecalidine and Pluviatilol can be seen in SD6. All the interaction details of best poses are mentioned in Table 4. To validate the docking result we have done molecular docking with the help of another docking software Pyrx also. The docking score for I-Asarinin by Pyrx is −10.8 kcal/mol (SD7). After the selection of the best poses for all the druglike molecules, we have to choose a bioactive ligand among all six which give the most stable complex structure. The docking results have concluded that I-Asarinin shows the best binding mode of interaction with minimum binding affinity score −10.8 kcal/mol. Moreover, the binding score obtained is far better than that of the most drugs presently used for the treatment of COVID-19. Drugs like chloroquine, favipiravir, hydroxychloroquine, interferon, and ribavirin which are widely given drugs to COVID-19 patients have binding scores of −7.0, −6,5, −7.2, −8.2 and −7.4 kcal/mol respectively which shows that I-Asarinin has the better potentiality to be used as drug-like compound against SARS-CoV-2. After I-Asarinin, the binding affinity score followed by Pluviatilol (−9.6 kcal/mol), Lignans Machilin F (−9.5 kcal/mol) and Aristololactum (−9.5 kcal/mol) is very near which reveals their good stability as a complex with the targeted PL^{pro} protease. I-Asarinin has the best binding affinity as compared to the other. This represent that I-Asarinin is the most potent inhibitor among all the considered ligands. To ensure the stability of biological complex we have also calculated the dipole moment of ligands. The high value of ligand dipole moment, shows the higher tendency to make stable complex with the macromolecule [54,55]. In the present case, the maximum value of dipole moment of 4.265Debye is observed for Fargesin. The value of dipole moment for I-Asarinin is 3.901Debye that is slightly less than that for Fargesin. This represent the stability of I-Asarinin: 4OVZ complex.

Our screening based on the best binding affinity score reveals that I-Asarinin shows the best potentiality to inhibit with PL^{pro} target. The first pose, which shows the maximum capability of bond formation with the target protein rather than the rest. It also validates I-Asarinin as the strong contender of a proposed drug against SARS-CoV-2. Moreover, the hydrogen-bond interactions play a vital role in stabilizing the target protein. Hydrogen-bond helps inbound the amino acids between polypeptide chains in protein structure. So, the larger the number of H-bond interactions present in protein, the more will be the binding affinity and though more stable the structure will be. The selected pose has the maximum number of H-bonds (including Conventional H-bonds, Carbon H-bonds, and Pi-donor H-bonds) showing the stability of the protein–ligand complex. Value for drieding energy for the selected pose is the second smallest succeeding that of the 4th pose with a negligible difference (Table 5).

Different possible interactions of protein–ligand complex and the donor–acceptor surface for the best pose (1) is shown in Fig. 3. I-Asarinin provide immune suppressive and hepato-protective (say, liver protection from damage) activities. It also exhibits several biological activities which helps in treatment of ovarian cancer in women [56] and in decreasing cholesterol levels [57]. It also has antihypertensive and antiangiogenic properties [58].

3.4. Molecular dynamics result analysis

MD analysis is a verified computer simulation method that is used for analyzing the physical movements of atoms and molecules and for obtaining dynamic data at atomic spatial resolution. Structures (say protein and complex) are optimized with minimum and negative potential energy and maximum force value. We have simulated Apo 4OVZ and I-asarinin-4OVZ complex for 100 ns to study the stability of the considered complex. The results obtained by performing MD simulations of Apo protein and protein–ligand complex are analyzed based on of values of H-bonds, the radius of gyration, RMSD, RSMF, and binding free energy. The mean and average values of different parameters are computed for the entire time trajectory and the results for both structures are compared (Table 6).

3.4.1. Hydrogen bond analysis

Despite being weaker than ionic and covalent bonds, intermolecular H-bonds predominantly contribute to complex formation. Therefore, H-bonds not only play a vital role in stabilizing the ligand with the protein structure but also helps in studying the drug specificity, accelerating metabolism and, adsorption. In the present study, we have observed that throughout the simulation time, complex I-Asarinin has a constant range of intermolecular H-bond interaction with receptor protein between 0 and 3 (Fig. 4). The average value of H-bond interaction seems to be 2

Table 5
Binding mode of each inhibitor-receptor pose of ligand I-Asarinin targeted on PL^{pro} protease of COVID-19.

S. no.	Binding affinity (Kcal/mol)	Drieding energy	Dipole moment	H-bond
1	−10.8	135.39	3.901	6
2	−10.2	148.63	2.808	4
3	−10.0	146.30	3.464	5
4	−9.5	131.03	4.387	2
5	−9.4	151.63	2.542	4
6	−9.0	141.16	4.471	3
7	−9.0	147.84	3.444	1
8	−8.9	150.41	3.779	4
9	−8.7	137.81	2.910	3

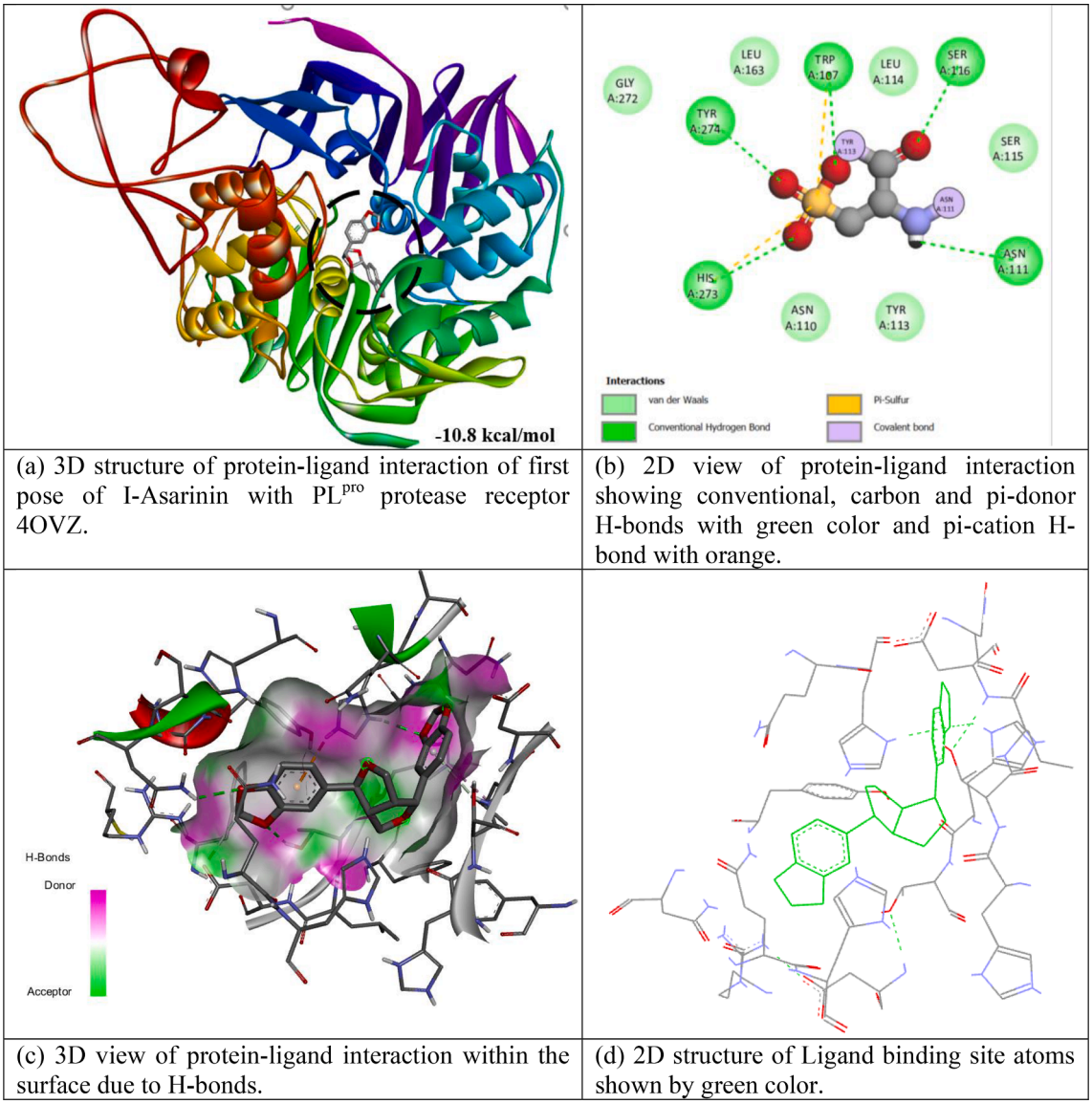

(a) 3D structure of protein-ligand interaction of first pose of I-Asarinin with PL^{pro} protease receptor 4OVZ.

(b) 2D view of protein-ligand interaction showing conventional, carbon and pi-donor H-bonds with green color and pi-cation H-bond with orange.

(c) 3D view of protein-ligand interaction within the surface due to H-bonds.

(d) 2D structure of Ligand binding site atoms shown by green color.

Fig. 3. Donor-acceptor interactions obtained by docking of I-Asarinin and receptor 4OVZ of PL^{pro} protease of COVID-19.

Table 6
MD Simulation output of time resolved trajectory of 4OVZ in its Apo state and in complex state with I-Asarinin for time trajectory from 0 ns to 100 ns.

S No.	Parameter	Apo 4OVZ		4OVZ + I-Asarinin complex	
		Mean	Range	Mean	Range
1.	Radius of gyration (nm)	23.81	23.585–24.05	24.535	23.79–25.08
2.	RMSD (nm)	2.89	2.5–3.37	3.74	2.5–4.86
3.	RMSF (nm)	1.906	0.591–3.85	2.65	0.636–6.48
4.	Calculated Binding energy (kcal/mol)	NA	NA	37.01	−58.5 to −11.9
5.	H-bond	NA	NA	0.403	0–3

(Table 6).

3.4.2. Radius of gyration (R_g)

R_g determines the compactness or compressed nature of protein and complex to time. Variation in R_g value reveals that Apo 4OVZ and protein show quite stable behavior throughout the simulation time trajectory. In this work, the variation of R_g for protein and protein–ligand complex have shown quite stable and compressed structures. The lesser the value of R_g more will be compactness and though more stable the complex will be. Without any major expansion, trajectories of Apo 4OVZ and protein–ligand complex have followed a steady path with an average value of 23.81 and 24.535 nm (Table 6). R_g value for complex structure is found to be ranging between 23.79 nm and 25.08 nm throughout the 100 ns of simulation exhibits the stability of both the protein and protein–ligand complex structure whereas the range of Apo 4OVZ structure is 23.585 nm to 24.05 nm (Table 6). Fig. 5 represents the graphical representation of total radius of gyration for Apo 4OVZ and 4OVZ-I-Asarinin complex.

3.4.3. Root mean square deviation (RMSD)

The RMSD values are calculated for the PL^{pro} Cα backbone of Apo-PL^{pro} and PL^{pro} complexed with I-Asarinin for 100 ns and are found to be in an acceptable range. Root mean square deviation (RMSD) value for the protein–ligand complex is seems to be proportionally increasing for the initial 25 ns of simulation process and later seem to be largely fluctuating between 3.25 and 4.5 nm. Whereas the RMSD trajectory of Apo protein is ranging from 2.5 nm to 3.37 nm (Table 6) but gradually increasing from 2.25 to 3.25 nm for the first 25 ns of the simulation and

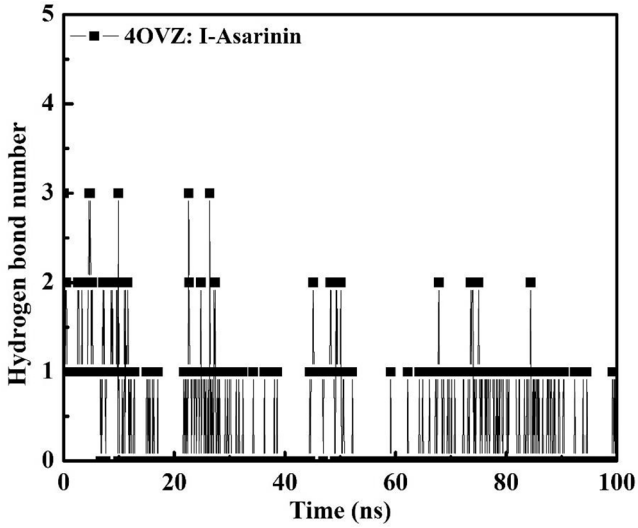

Fig. 4. Intermolecular H-bond numbers between I-Asarinin and protein–ligand complex for time trajectory from 0 ns to 100 ns.

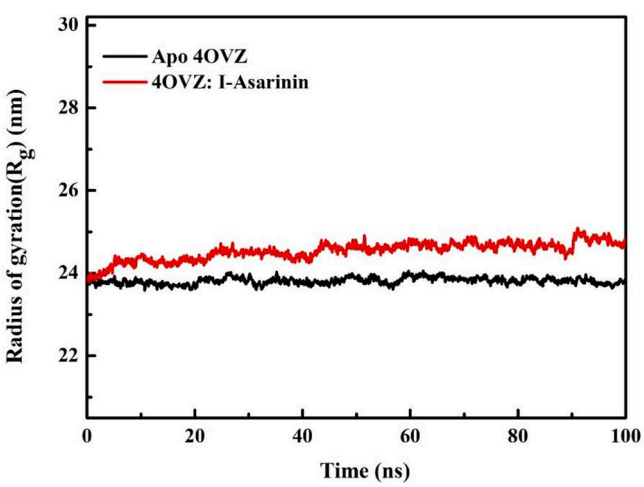

Fig. 5. Total Radius of Gyration for Apo 4OVZ and 4OVZ-I-Asarinin complex for time trajectory from 0 ns to 100 ns.

then fluctuates between 2.50 and 3.25 nm (Fig. 6). Protein-ligand complex displayed a little high value for RMSD as compared to Apo 4OVZ. The obtained average RMSD value of complex i.e., 3.74 nm is found to be slightly higher than that of protein structure which is 2.89 nm. The variation of 0.85 nm is found to be in between both the average values of RMSDs which is expected because position restraints can never be fully perfect for energy minimized structures.

3.4.4. Root mean square fluctuations (RMSF)

Unlike RMSD trajectories, the counterplots of RMSF show high fluctuations throughout the simulation time. RMSF give an account of heterogeneity and the steady-state of macromolecule. In simple words, RMSF suggests the stability of all active and flexible protein residues. RMSF data from Fig. 7 shows the highest peaks of fluctuation of the 4OVZ-I-Asarinin complex in between 250 and 300 residues and RMSF range 0.636 to 6.48 nm (Table 6) with the highest peak value 6.48 nm. The average for the entire trajectory of the complex is computed at 2.65 nm. Whereas the simulated RMSF graph of Apo 4OVZ shows four times major peak fluctuations from 100 to 300 residue numbers. With an average RMSF value of 1.906 nm, trajectory for Apo 4OVZ fluctuates between 0.591 and 3.85 nm (Table 6).

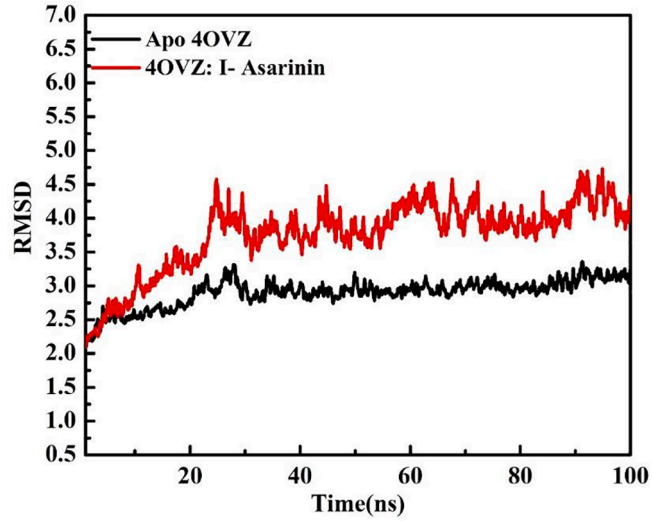

Fig. 6. Root Mean Square Deviation graphs of 4OVZ in Apo state and its complex with I-Asarinin for time trajectory from 0 ns to 100 ns.

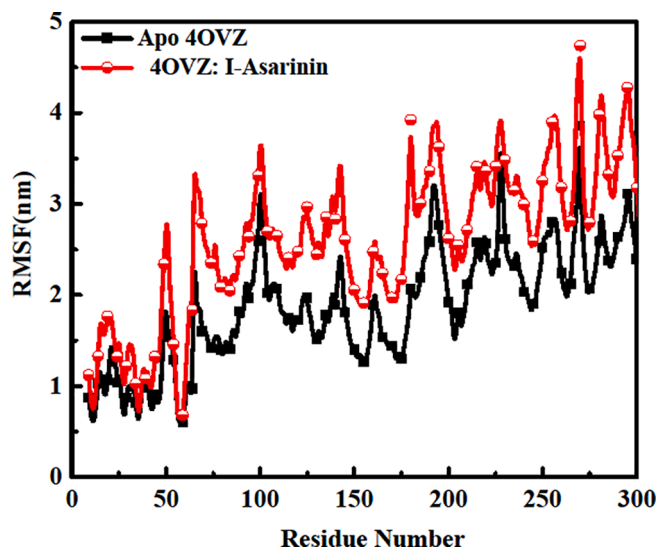

Fig. 7. Root Mean Square Fluctuations graphs of 4OVZ in Apo state and its complex with I-Asarinin for time trajectory from 0 ns to 100 ns.

From all the values of RMSD and RMSF, we can say that the protein backbone of 4OVZ remains unaltererd by the presence of I-Asarinin. The structure of protease PL^{pro} is not much disturbed.

3.4.5. Calculated binding energy

Fig. 8 shows the calculated binding energy curve for the binding of drug-like molecule I-Asarinin with PL^{pro} protease. It shows the extend of binding of a considered ligand with the preferred protein. Graphical data shows that the curve has the highest calculated binding energy of −11.9 kcal/mol in frame 190. The average calculated binding energy of trajectory is −37.018 kcal/mol ranging from −57.10 kcal/mol to −11.949 kcal/mol validates the stability of I-Asarinin-4OVZ complex (Table 6).

4. Conclusion

Traditional plants have been considered as the rich source of ailments for various diseases. For this study, we have considered some phytochemicals extracted from a specific plant *Piper Longum,* which is a

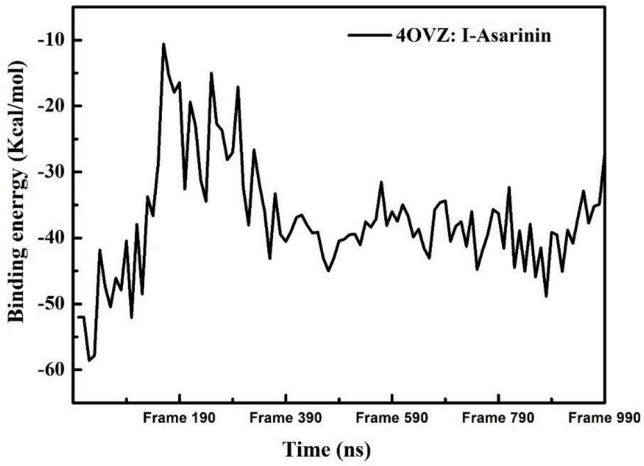

Fig. 8. Graphical representation showing binding free energy for protein–ligand complex for time trajectory from 0 ns to 100 ns.

proven medicinal plant since ancient times. On the other hand, an essential drug against SARS-CoV-2 is a must. With the help of this work, we have tried to summarize different computational techniques done on phytochemicals of plant *Piper Longum* targeting PL^{pro} protease of COVID-19. Molecular docking has revealed that I-Asarinin, a component of *Piper Longum* with the best binding affinity score of −10.8 kcal/mol and following most of the ADMET properties, has forced us to assume it is a better component to be used as a drug against COVID-19. Furthermore, the MD Simulation results have justified our assumption by showing acceptable values of calculated binding energy. H-bond interactions and radius of gyration although, explained the better stability and compactness of protein itself. Comparison in complex and Apo 4OVZ for RMSD and RMSF values determines that simulation has not highly disturbed the structures of complex and Apo 4OVZ. All these properties uplift our motive to use I-Asarinin as a potential drug against COVID-19 and we truly believe that this in-silico study will lead to drug development for the treatment of COVID-19.

CRediT authorship contribution statement

Shradha Lakhera: Data curation, Writing – original draft, Visualization, Investigation, Software, Validation. **Kamal Devlal:** Conceptualization, Writing - review & editing. **Arabinda Ghosh:** Data curation, Software, Validation. **Meenakshi Rana:** Conceptualization, Methodology, Writing - review & editing, Supervision.

Declaration of Competing Interest

The authors declare that they have no known competing financial interests or personal relationships that could have appeared to influence the work reported in this paper.

Appendix A. Supplementary data

Supplementary data to this article can be found online at https://doi.org/10.1016/j.rechem.2021.100199.

References

[1] WHO (World Health Organisation) weekly epidemiological update https://www.who.int/publications/m/item/weekly-epidemiological-update-on-COVID-19—18-may-2021.
[2] K.N. Sunil Kumar, K.G. Divya, R. Mattummal, B. Erni, P. Sathiyarajeswaran, K. Kanakavalli, Pharmacological Actions of Contents of Kabasura Kudineer- A Siddha Formulation for Fever with Respiratory Illness, Indian J. Pharm. Educ. 55 (1) (2021) 36–55, https://doi.org/10.5530/ijper10.5530/ijper.55.110.5530/ijper.55.1.7.
[3] A.E. Gorbalenya, S.C. Baker, The species severe acute respiratory syndrome-related coronavirus: classifying 2019-nCoV and naming it SARS-CoV-2, Nat. Microbiol. 5 (4) (2020) 536–544, https://doi.org/10.1038/s41564-020-0695-z.
[4] J.S. Mackenzie, D.W. Smith, COVID-19: a novel zoonotic disease caused by a coronavirus from China: what we know and what we don't, Microbiology 41 (2020) 45–50, https://doi.org/10.1071/MA20013.
[5] S. Asadi, N. Bouvier, A.S. Wexler, W.D. Ristenpart, The coronavirus pandemic and aerosols: Does COVID-19 transmit via expiratory particles? Aerosol. Sci. Technol. 54 (6) (2020) 635–638, https://doi.org/10.1080/02786826.2020.1749229.
[6] S. Koyama, R. Ueha, K. Kondo, Loss of Smell and Taste in Patients with Suspected COVID-19: Analyses of Patients' Reports on Social Media, J. Med. Internet Res. 23 (4) (2021) 26459, https://doi.org/10.2196/26459.
[7] P.S. Eun, Epidemiology, virology, and clinical features of severe acute respiratory syndrome -coronavirus-2 (SARS-CoV-2; Coronavirus Disease-19), Clin. Exp. Pediatr. 63 (4) (2020) 119–124, https://doi.org/10.3345/cep.2020.00493.
[8] S.A. Meo, I.A. Bukhari, J.A.S. Meo, D.C. Klonoff, Comparison of biological, pharmacological characteristics and adverse effects of Pfizer/BioNTech and Moderna Vaccines, Eur. Rev. Med. Pharmacol. Sci. 25 (2021) 1663–1669. https://www.europeanreview.org/wp/wp-content/uploads/1663-1669.pdf.
[9] P. McIntyre, Y.J. Joo, C. Chiu, K. Flanagan, K. Macartney, COVID-19 vaccines -are we there yet? Australian Prescriber. 44 (1) (2021) 19–25, https://doi.org/10.18773/austprescr.2020.084.
[10] D.M. Zuckerman, Emergency Use Authorizations (EUAs) Versus FDA Approval: Implications for COVID-19 and Public Health, Am. J. Public Health 111 (6) (2021) 1065–1069, https://doi.org/10.2105/AJPH.2021.306273.
[11] B.J. Oso, A. Oluwaseun, Adeoye, I.F. Olaoye, Pharmacoinformatics and hypothetical studies on allicin, curcumin, and gingerol as potential candidates against COVID-19-associated proteases, J. Biomol. Struct. Dyn. (2020). https://doi.org/10.1080/07391102.2020.1813630.
[12] Manish Kumar Tripathi, Pushpendra Singh, Sujata Sharma, Tej P. Singh, A. S. Ethayathulla, Punit Kaur, Identification of bioactive molecule from Withania somnifera (Ashwagandha) as SARS-CoV-2 main protease inhibitor, J. Biomol. Struct. Dyn. 39 (15) (2021) 5668–5681, https://doi.org/10.1080/07391102.2020.1790425.
[13] Rupesh V. Chikhale, Shailendra S. Gurav, Rajesh B. Patil, Saurabh K. Sinha, Satyendra K. Prasad, Anshul Shakya, Sushant K. Shrivastava, Nilambari S. Gurav, Rupali S. Prasad, SARS-CoV-2 host entry and replication inhibitors from Indian ginseng: an in-silico approach, J. Biomol. Struct. Dyn. 39 (12) (2021) 4510–4521, https://doi.org/10.1080/07391102.2020.1778539.
[14] P. Chowdhury, In silico investigation of phytoconstituents from Indian medicinal herb 'Tinospora cordifolia (giloy)' against SARS-CoV-2 (COVID-19) by molecular dynamics approach, J. Biomol. Struct. Dyn. (2020), https://doi.org/10.1080/07391102.2020.1803968.
[15] Pratik Das, Ranabir Majumder, Mahitosh Mandal, Piyali Basak, In-Silico approach for identification of effective and stable inhibitors for COVID-19 main protease (Mpro) from flavonoid based phytochemical constituents of Calendula officinalis, J. Biomol. Struct. Dyn. 39 (16) (2021) 6265–6280, https://doi.org/10.1080/07391102.2020.1796799.
[16] C. Mouffouk, S. Mouffouk, S. Mouffouk, L. Hambaba, H. Habab, Flavonols as potential antiviral drugs targeting SARS-CoV-2 proteases (3CLpro and PLpro), spike protein, RNA-dependent RNA polymerase (RdRp) and angiotensin-converting enzyme II receptor (ACE2), Eur. J. Pharmacol. 891 (2020) 173759. https://doi.org/10.1016/j.ejphar.2020.173759.
[17] M. Kandeel, M. Al-Nazawi, Virtual screening and repurposing of FDA approved drugs against COVID-19 main protease, Life Sci. 15 (251) (2020) 117627, https://doi.org/10.1016/j.lfs.2020.117627.
[18] M. Zmudzinski, M. Rut, G. Olech, J. Granda, M. Giurg, M.B. Grabowska, L. Zhang, X. Sun, L. Zongyang, D. Nayak, M.K. Brodacka, S.K. Olsen, R. Hilgenfeld, M. Drag, Ebselen derivatives are very potent dual inhibitors of SARS-CoV-2 proteases - PLpro and Mpro in vitro studies, bioRxiv (2020), https://doi.org/10.1101/2020.08.30.273979.
[19] Claudio N. Cavasotto, Juan I. Di Filippo, In silico Drug Repurposing for COVID-19: Targeting SARS-CoV-2 Proteins through Docking and Consensus Ranking, Mol. Inform. 40 (1) (2021) 2000115, https://doi.org/10.1002/minf.v40.110.1002/minf.202000115.
[20] N. Barretto, D. Jukneliene, K. Ratia, Z. Chen, A.D. Mesecar, S. C. Baker, The Papain-Like Protease of Severe Acute Respiratory Syndrome Coronavirus Has Deubiquitinating Activity, J. Viro. 79(24) (2005) 15189–15198. https://doi.org/10.1128/JVI.79.24.15189-15198.2005.
[21] T.D., Structure of SARS CoV2. In: Nanotechnology-COVID-19 Interface, Springer Briefs Appl. Sci. Technol. (2021) 11–24. https://doi.org/10.1007/978-981-33-6300-7_2.
[22] Nabajyoti Baildya, Abdul Ashik Khan, Narendra Nath Ghosh, Tanmoy Dutta, Asoke P. Chattopadhyay, Screening of potential drug from Azadirachta Indica (Neem) extracts for SARS-CoV-2: An insight from molecular docking and MD-simulation studies, J. Mol. Struct. 1227 (2021) 129390, https://doi.org/10.1016/j.molstruc.2020.129390.
[23] Sk Saruk Islam, Sujoy Midya, Sanjit Sinha, Sk Md Abu Imam Saadi, Natural medicinal plant products as an immune-boosters: A possible role to lessen the impact of COVID-19, Case Stud. Chem. Environ. Eng. 4 (2021) 100105, https://doi.org/10.1016/j.cscee.2021.100105.
[24] R. Yadav, J.K. Chaudhary, N. Jain, P. Chaudhary, S. Khanra, P. Dhamija, A. Sharma, A. Kumar, S. Handu, Role of Structural and Non-Structural Proteins and Therapeutic Targets of SARS-CoV-2 for COVID-19, MDPI 10 (4) (2021) 821, https://doi.org/10.3390/cells10040821.

[25] L. Mengxia, G. Ye, Y. Si, Z. Shen, L. Liu, Y. Shi, S. Xiao, Z.F. Fu, G. Peng, Structure of the multiple functional domains from coronavirus nonstructural protein 3, Emerg. Microb. Infect. 10 (1) (2021) 66–80, https://doi.org/10.1080/22221751.2020.1865840.

[26] Y.S. Wijayasinghe, P. Bhansali, R. Viola, M.A. Kamal, N.K. Poddar, Natural Products: A Rich Source of Antiviral Drug Lead Candidates for the Management of COVID-19, Current Pharmaceutical Design, Bentham Science Publishers, 2021, p. 26.

[27] C.N. Cavasotto, M.S. Lamas, J. Maggini, Functional and druggability analysis of the SARS-CoV-2 proteome", Eur. J. Pharmacol. 5 (890) (2021 Jan) 173705, https://doi.org/10.1016/j.ejphar.2020.173705.

[28] T.P. Kumar, J. Karihaloo, S. Archak, Analysis of genetic diversity in Piper nigrum L. using RAPD markers, Genet. Resour. Crop Evol. 50 (2003) 469–475, https://doi.org/10.1023/A:1023917809042.

[29] S. Kumar, J. Kamboj, S.S. Sharma, Overview for Various Aspects of the Health Benefits of Piper Longum Linn. Fruit, J. Acupunct. Meridian Stud. 4(2) (2011) 134–140. https://doi.org/10.1016/S2005-2901(11)60020-4.

[30] R. Sharma, N. Kumari, M.S. Ashawat, C.P.S. Verma, Zingiber officinalis, Rosc., Curcuma longa Linn., Cinnamonum zeylanicum Nees., Piper longum, Linn., Boerhaavia diffussa Linn, AJPTech. 10 (2020) 3, https://search.proquest.com/openview/335b2b049931412b065e81baf26bdec9/1?pq-origsite=gscholar&cbl=2044946.

[31] Shahin Moradi, Namdar Yousofvand, Peganum Harmala and Piper Longum Plant Rubbing Oil Effect on Pain in Small Male Mice, Biosci. Biotech. Res. Asia 13 (2) (2016) 821–826.

[32] A. Khandhar, S. Patel, A. Patel, M. Zaveri, Chemistry and pharmacology of Piper Longum L, Int. J. Pharm. Sci. Rev. Res. 5 (2010) 67–76. https://www.researchgate.net/publication/257299404_Chemistry_and_pharmacology_of_Piper_Longum_L.

[33] Dr. A.D. Ashok, J. Ravivarman, Dr. K. Kayalvizhi, Nutraceutical properties of recommended horticultural crops to develop human immune system against COVID-19, Int. J. Chem. Stud. 8 (4) (2020) 105–112.

[34] E.S. Sunila, G. Kuttan, Immunomodulatory and antitumor activity of Piper longum Linn. and piperine, J. Ethnopharmacol. 90(2–3) (2004) 339–346. https://doi.org/10.1016/j.jep.2003.10.016.

[35] Srivastava Niraj, Saxena Varsha, Plant Science Today; A review on scope of immuno-modulatory drugs in Ayurveda for prevention and treatment of COVID-19, Plant Sci. Today 7 (3) (2020) 417–423.

[36] Noel M O'Boyle, Michael Banck, Craig A James, Chris Morley, Tim Vandermeersch, Geoffrey R Hutchison, Open Babel: An open chemical toolbox, J. Cheminform. 3 (1) (2011), https://doi.org/10.1186/1758-2946-3-33.

[37] M.A. Hammed, I.O. Adedotun, A.F. Victoria, Adewusi, J. Adepoju, S.B. Olasupo, M. W. Akinboade, Target-Based Drug Discovery, ADMET Profiling and Bioactivity Studies of Antibiotics as Potential Inhibitors of SARS-CoV-2 Main Protease (Mpro), Research square. (2021). https://www.researchsquare.com/article/rs-310136/latest.pdf.

[38] C.A. Lipinski, Lead- and drug-like compounds: The rule-of-five revolution, Drug Discov. Today Technol. 1 (4) (2004) 337–341, https://doi.org/10.1016/j.ddtec.2004.11.007.

[39] K.M. Giacomini, S.M. Huang, D.J. Tweedie, L.Z. Benet, K.L. Brouwer, X. Chu, A. Dahlin, R. Evers, V. Fischer, K.M. Hillgren, K.A. Hoffmaster, T. Ishikawa, D. Keppler, R.B. Kim, C.A. Lee, M. Niemi, J.M. Polli, Y. Sugiyama, P.W. Swaan, L. Zhang, Membrane transporters in drug development, Nat. Rev. Drug Discov. 9 (3) (2010) 215–236, https://doi.org/10.1038/nrd3028.

[40] D.F. Veber, S.R. Johnson, H.Y. Cheng, B.R. Smith, K.W. Ward, K.D. Kopple, Molecular Properties That Influence the Oral Bioavailability of Drug Candidates, J. Med. Chem. 45 (12) (2002) 2615–2623, https://doi.org/10.1021/jm020017n.

[41] S. Shahab, M. Sheikhi, R. Alnajjar, S.A. Saud, M. Khancheuski, A. Strogova, DFT investigation of atazanavir as potential inhibitor for 2019-nCoV coronavirus M protease, J. Mol. Struct. 1228 (2021) 1461, https://doi.org/10.1016/j.molstruc.2020.129461.

[42] Mohd Athar, Mohsin Y. Lone, Prakash C. Jha, Designing of calixarene based drug carrier for dasatinib, lapatinib and nilotinib using multilevel molecular docking and dynamics simulations, J. Incl. Phenom. Macrocycl. Chem. 90 (1-2) (2018) 157–169, https://doi.org/10.1007/s10847-017-0773-x.

[43] S. Deb, A.A. Reeves, R. Hopefl, R. Bejusca, ADME and pharmacokinetic properties of remdesivir: its drug interaction potential, Pharmaceuticals 14 (7) (2021) 655, https://doi.org/10.3390/ph14070655.

[44] F. Cheng, W. Li, Y. Zhou, J. Shen, Z. Wu, G. Liu, P.W. Lee, Y. Tang, A Comprehensive Source and Free Tool for Assessment of Chemical ADMET Properties, ACS Publication Chem. Inf. Model. 52 (2012) 3099–3105, https://doi.org/10.1016/j.molstruc.2017.09.108.

[45] J.B. Baell, The American Chemical Society and American Society of Pharmacognosy; Feeling Nature's PAINS: Natural Products, Natural Product Drugs, and Pan Assay Interference Compounds (PAINS), J. Nat. Prod. 79 (3) (2016) 616–628, https://doi.org/10.1021/acs.jnatprod.5b00947.

[46] J.B. Baell, J.W.M. Nissink, Seven Year Itch: Pan-Assay Interference Compounds (PAINS) in Utility and Limitations, ACS Chem. Bio. 13 (1) (2017) 36–44, https://doi.org/10.1021/acschembio.7b00903.

[47] Priya Antony, Ranjit Vijayan, Jie Zheng, Identification of Novel Aldose Reductase Inhibitors from Spices: A Molecular Docking and Simulation Study, PLOS ONE 10 (9) (2015) e0138186, https://doi.org/10.1371/journal.pone.0138186.10.1371/journal.pone.0138186.g00110.1371/journal.pone.0138186.g00210.1371/journal.pone.0138186.g00310.1371/journal.pone.0138186.g00410.1371/journal.pone.0138186.g00510.1371/journal.pone.0138186.t00110.1371/journal.pone.0138186.t00210.1371/journal.pone.0138186.t00310.1371/journal.pone.0138186.s00110.1371/journal.pone.0138186.s00210.1371/journal.pone.0138186.s00310.1371/journal.pone.0138186.s00410.1371/journal.pone.0138186.s00510.1371/journal.pone.0138186.s00610.1371/journal.pone.0138186.s00710.1371/journal.pone.0138186.s00810.1371/journal.pone.0138186.s00910.1371/journal.pone.0138186.s01010.1371/journal.pone.0138186.s011.

[48] O. Trott, A.J. Olson, AutoDock Vina: improving the speed and accuracy of docking with a new scoring function, efficient optimization, and multithreading, J. Comput. Chem. 31 (2) (2009) 455–461, https://doi.org/10.1002/jcc.21334.

[49] S. Dallakyan, A.J. Olson, Small-Molecule Library Screening by Docking with PyRx, Chem. Bio. (2015) 1263. https://link.springer.com/protocol/10.1007/978-1-4939-2269-7_19.

[50] B.V. Bhaskar, T.M. Babu, N.V. Reddy, W. Rajendra, Homology modeling, molecular dynamics, and virtual screening of NorA efflux pump inhibitors of Staphylococcus aureus, Drug Des. Devel. Ther. 10 (2016) 3237–3252, https://doi.org/10.2147/DDDT.S113556.

[51] F. Faassen, G. Vogel, H. Spanings, H. Vromans, Caco-2 permeability, P glycoprotein transport ratios and brain penetration of heterocyclic drugs, Int. J. Pharm. 263 (2003) 113–122, https://doi.org/10.1016/S0378-5173(03)00372-7.

[52] Jason A. Roberts, Federico Pea, Jeffrey Lipman, The Clinical Relevance of Plasma Protein Binding Changes, Clin. Pharmacokin. 52 (1) (2013) 1–8, https://doi.org/10.1007/s40262-012-0018-5.

[53] Katja Hansen, Sebastian Mika, Timon Schroeter, Andreas Sutter, Antonius ter Laak, Thomas Steger-Hartmann, Nikolaus Heinrich, Klaus-Robert Müller, Benchmark Data Set for in Silico Prediction of Ames Mutagenicity, A. C. S. Publication 49 (9) (2009) 2077–2081, https://doi.org/10.1021/ci900161g.

[54] M. Kouza, A. Banerji, A. Kolinski, I. Buhimschi, A. Kloczkowski, Role of Resultant Dipole Moment in Mechanical Dissociation of Biological Complexes, Molecules 23 (8) (2018) 1995, https://doi.org/10.3390/molecules23081995.

[55] F. Beierlein, H. Lanig, G. Schurer, H. Anselm, C. Horn, T. Clark, Quantum mechanical/molecular mechanical (QM/MM) docking: an evaluation for known test systems, Mol. Phys. 101 (15) (2003) 2469–2480, https://doi.org/10.1080/0026897031000092940.

[56] C. Chen, X. Shi, T. Zhou, W. Li, S. Li, G. Bai, Full-length transcriptome analysis and identification of genes involved in asarinin and aristolochic acid biosynthesis in medicinal plant Asarum sieboldii, Genome 64 (6) (2020) 639–653, https://doi.org/10.1139/gen-2020-0095.

[57] M. Yingyan, X. Kai, S. Wang, Y. Han, Simultaneous Determination of Two Epimeric Furofuran Lignans (Sesamin and Asarinin) of Asarum heterotropoides Extract in Rat Plasma by LC/MS/MS; Application to Pharmacokinetic Study, Chromatogr. Sci. 52 (8) (2013) 793–798, https://doi.org/10.1093/chromsci/bmt114.

[58] M. Jeong, H.M. Kim, J.S. Lee, J.H. Choi, D.S. Jang, (−)-Asarinin from the Roots of Asarum sieboldii Induces Apoptotic Cell Death via Caspase Activation in Human Ovarian Cancer Cells, Molecules 23 (8) (2018) 1849, https://doi.org/10.3390/molecules23081849.